Magazine of Civil Engineering

journal homepage: http://engstroy.spbstu.ru/

ISSN 2071-0305

DOI: 10.18720/MCE.87.3

Bearing capacity of fastener steel tube full hall scaffolds

Z. Lu*, G. Chao,
Shenyang Jianzhu University, Shenyang City, Liaoning, P.R.China
** E-mail: luzhengranglovel@126.com*

Keywords: fastener steel tube full hall scaffold, eccentric axial load, bearing capacity, failure mode, nonlinear finite element analysis.

Abstract. In fastener steel tube full hall scaffolds (FSTFHSs), the upper load is transferred to the posts through the top horizontal tubes. Further, the posts and horizontal tubes are not always in the same plane owing to the eccentricity of the coupler connections. Moreover, building materials and construction machinery are usually eccentrically stacked atop the FSTFHSs. Therefore, the members in FSTFHSs are subject to eccentric axial loading. This paper reports a systematic experimental and analytical study on the bearing capacity of FSTFHSs with eccentric axial loads on the tubes. Five full-scale FSTFHS specimens were built and tested for failure to obtain the strength and failure modes of FSTFHSs whose members are subject to eccentric axial loads. Advanced nonlinear finite element analysis (FEA) was conducted on the specimen models to obtain the strength and failure modes of the FSTFHS under eccentric axial load of the member and to compare with the experimental results. Parametric studies were conducted based on the FEA results to investigate the influence of eccentric axial loads on the bearing capacity of FSTFHSs with different geometric properties. The experimental and analytical results show that eccentric axial loading negatively affects the FSTFHS bearing capacity and that the main failure mode of FSTFHS is the local instability of the posts in the heaped load areas, accompanied by the twisting of the entire structure and bending of the top horizontal tubes.

1. Introduction

Fastener steel tube full hall scaffold (FSTFHS) systems are widely used as temporary structures in concrete casting construction, which involves the management of large loads (e.g. construction of girders and continuous box girder bridges), owing to their ease in fabrication, installation, and dissemination. However, FSTFHS systems have collapsed in many places (Figure 1), resulting in many casualties [1–4].

Figure 1. Collapse of FSTFHS system during construction in Yunnan Province on January 3, 2010.

Lu, Z.., Chao, G. Bearing capacity of fastener steel tube full hall scaffolds. Magazine of Civil Engineering. 2019. 87(3). Pp. 35–45. DOI: 10.18720/MCE.87.3.

Лу Ч., Чао Г. Несущая способность крепёжной стальной трубы строительных лесов // Инженерно-строительный журнал. 2019. № 3(87). С. 35–45. DOI: 10.18720/MCE.87.3

An FSTFHS system comprises three or more rows of vertical posts connected by couplers, horizontal tubes, and X-bracing. Depending on the load-transfer modes, such system can be classified as either fastener steel tube full hall formwork support (FSTFHFS, Figure 2) or FSTFHS (Figure 3). In FSTFHFS, the load is directly transferred to the posts through adjustable U-heads. However, in FSTFHS, the load is first transferred to the top horizontal tubes through wood braces or scaffold boards, which then transfer the load to the posts. The distance between the resultant action point of upper load and the neighbouring post is expressed as eccentricity e, as shown in Figure 3. This load-transfer mode has eccentricity [5–7]. The difference between the FSTFHFS and FSTFHS is really worthy of study to determine the influence of the eccentric load-transfer mode on the critical load of the system. Furthermore, all tubes are connected using couplers whose centre lines are not always in the same plane (Figure 4). Moreover, building materials and construction machinery are usually eccentrically stacked atop FSTFHSs (Figure 5). These loading conditions mean that the members of an FSTFHS are subject to eccentric axial loads, which might cause part of the posts to buckle due to overloading, consequently resulting in the collapse of the FSTFHS.

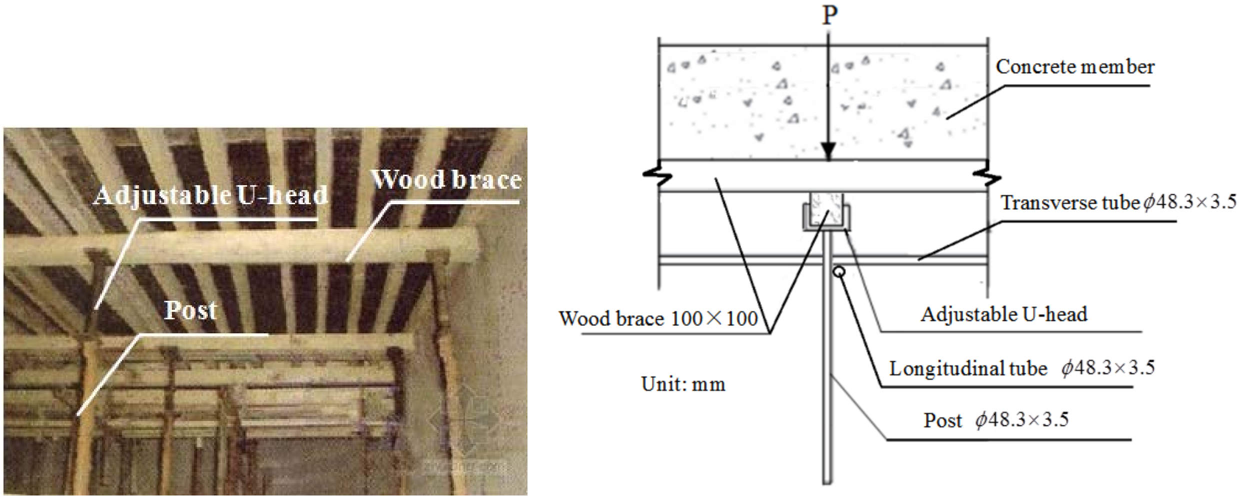

Figure 2. Load transfer through adjustable U-head in FSTFHFS.

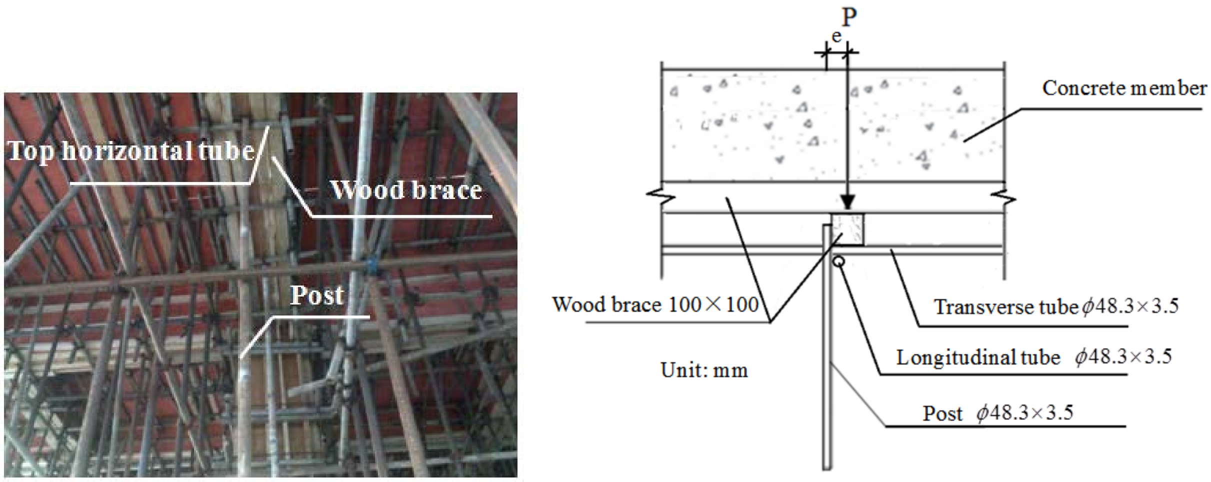

Figure 3. Load transfer through top horizontal tube in FSTFHS.

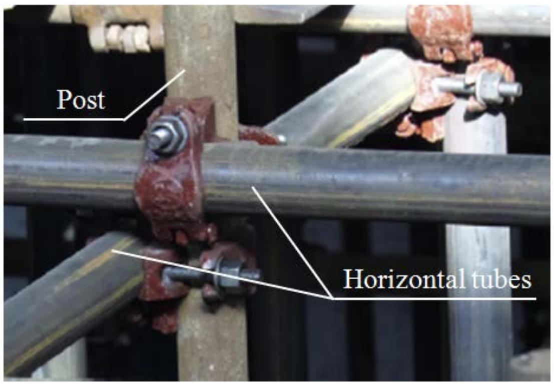

Figure 4. Eccentricity induced by connection of right-angle coupler.

Figure 5. Eccentric local heaped load.

Many studies on FSTFHFS have been conducted since the 2000s. Yuan [8], Hu [9], and Xie [10] have performed reliability analyses of FSTFHFS. Beale [11–13], Ao [14], Yue [15], and Liu [16, 17] have published numerous experimental and theoretical studies on the stability capacity and the design method of FSTFHFS. Similarly, systematic studies [18–20] have also been conducted on the bearing capacity and design method of FSTFHFS, including 12 FSTFHFS prototype tests and several finite element analyses (FEAs). In contrast, FSTFHSs, which are used in the construction of large-span spatial structures such as gymnasiums, train stations, garages, and bridges, have been scarcely investigated. In addition, using the above-mentioned research results in which the member eccentric axial loads are neglected is inaccurate and inappropriate in designing FSTFHSs. Disastrous collapse of FSTFHS has occurred in several countries, which casts doubt on the safety of such systems. Understanding the structural behaviour of FSTFHS through experimental and theoretical studies is essential to prevent such collapse.

This work aims to conduct experimental and theoretical studies to investigate the following: (1) the bearing capacity and failure modes of several different FSTFHSs with eccentric axial loads on tubes, (2) the effect of setting parameters and loading conditions on the FSTFHSs, and (3) the effect of eccentric axial load on the bearing capacity of the FSTFHSs with various geometric properties.

2. Methods

2.1. Experimental Investigation

All steel members and couplers used in the tests were obtained from actual construction sites. The steel tubes used in the test specimens had a diameter of 48.3 mm and a thickness of 3.02 mm. Three randomly selected steel tubes were processed into arc-shaped work pieces in accordance with code GB/T228-2002[21] as shown in Figure 6(a) for material testing. The test specimen was fixed on the tensile testing machine (Figure 6(b)). Figure 6(c) shows the corresponding tensile curves. The average yield strength, ultimate strength, and Young's modulus E of the steel tubes were 374.92 MPa, 436.92 MPa, and 184 GPa, respectively.

(a)Three arc-shaped test specimens

(b) Test specimen fixed on the tensile testing machine

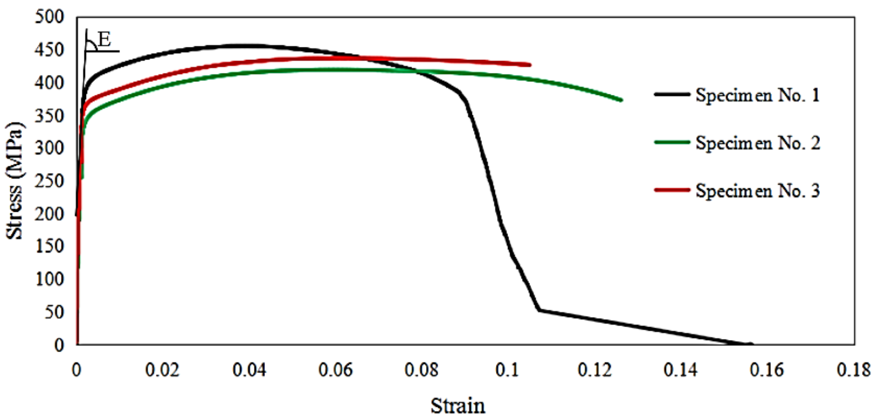

(c) Tensile curves

Figure 6. Tensile curves of the materials.

Building materials are usually eccentrically stacked atop FSTFHSs, meaning that they are subject to large eccentric local heaped loads. Thus, two loading methods were adopted in the tests: uniform load over the entire FSTFHS [hereinafter referred to as whole area load, Figure 7(a)] and uniform load over local regions on the FSTFHS [hereinafter referred to as local area load, Figure 7(b)].

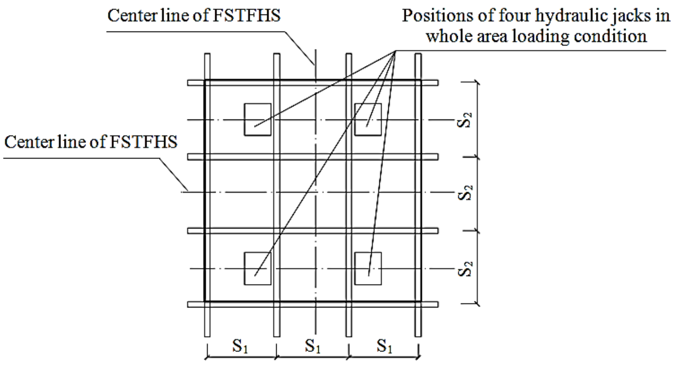

(a) Loading Method in the Whole Area Load Condition

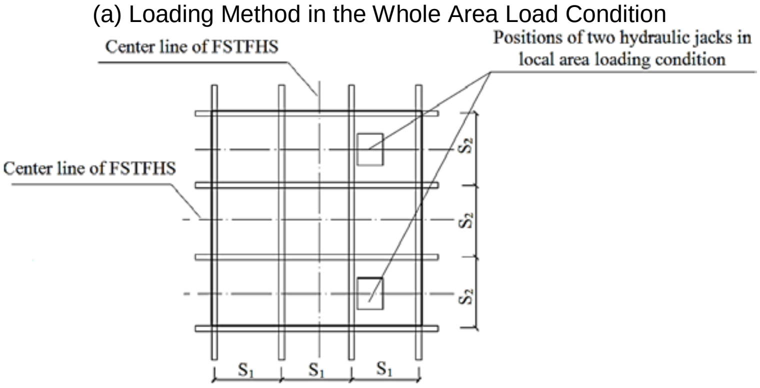

(b) Loading method in the local area load condition

Note: (a) and (b) show the plans of the test specimens without X-bracing under the whole and local area load conditions, respectively, and the thick solid lines indicate the planes with vertical X-bracing.

Figure 7. Placement of the hydraulic jacks in the two loading methods.

Loading frames, four 50-ton hydraulic jacks (two in the local area load condition), and two layers of steel distribution beams were used in the tests. Vertical uniform loads were applied at the top horizontal tubes of the FSTFHS in the specified loading area as follows: the hydraulic jacks were fastened to the bottom of girders in the loading frames, and vertical loads were applied to the top-layer distribution beams. The loads were then transferred to a group of bottom distribution beams in the perpendicular direction and finally to the FSTFHS. Figures 8 and 9 show the test setup and general layout of the test specimens, respectively.

The multistage loading method where loads were applied in increments of 20 kN for 3 min each was adopted in the tests. When the applied total load approached the anticipated bearing capacity computed using the JGJ 130–2011 code [22], the load step increment was reduced to 2 kN with each step load applied until the strain and displacement stabilized. For safety purposes, the specimens were not loaded until the collapse. The pressure in the hydraulic jacks decreased when the FSTFHS specimens reached their peak load and started to unload owing to instability. At this point, the specimens were considered to have failed, and thus, the test was stopped.

2.2. Numerical Investigation

A nonlinear analysis was performed using the FEA software ANSYS to study the behaviour and predict the strength of the FSTFHS test specimens. To simulate the semi-rigid behaviour of the right-angle couplers, spring-damper element (COMBIN14) with a spring constant of 19.0 kN·m/rad–the mean initial rotational stiffness obtained from earlier right-angle coupler tests [23]–was used in the analysis.

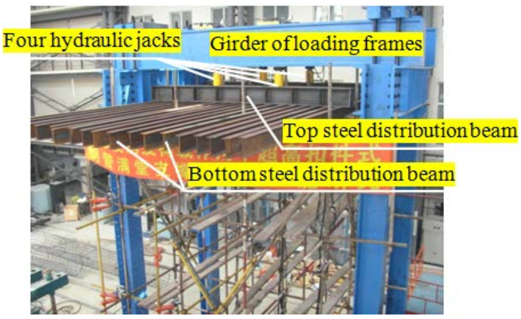

(a) Test setup under the whole area load condition

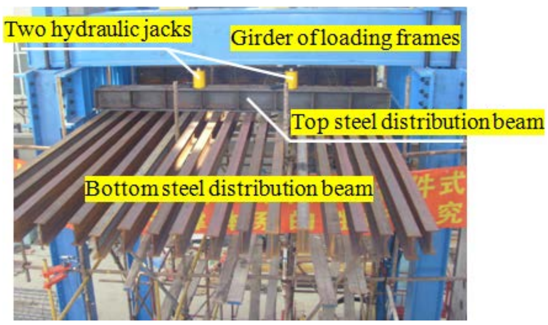

(b) Test setup under the local area load condition

Figure 8. Test setup.

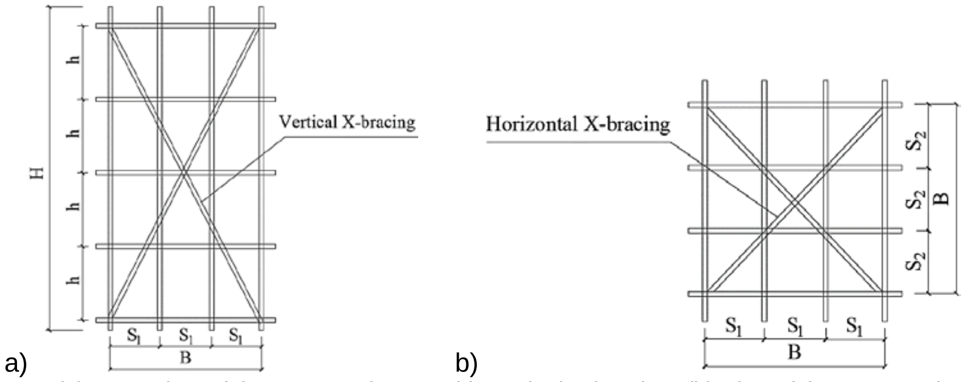

Note: (a) Front view of the test specimens with vertical X-bracing. (b) Plan of the test specimens with horizontal X-bracing.

Figure 9. General layout of the FSTFHS.

In the FSTFHS, longitudinal and transverse horizontal tubes are connected to the posts using right-angle couplers (Figure 10), and the X-bracing members are connected to the posts or horizontal tubes using swivel couplers (Figure 11). The centre lines of all connected tubes may not be in the same plane but are at a certain eccentric distance. This eccentric distance was set to 53 mm in the FEA as shown in Figure 10. The main node (Figure 12) was the intersection between a post and two tubes in the perpendicular directions, and the vertical distance between the nodes connecting the two tubes in different directions was set to 150 mm.

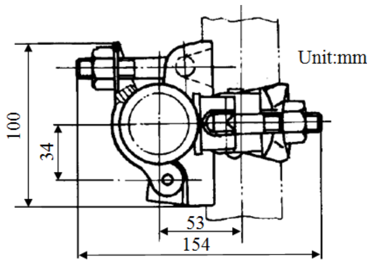

Figure 10. Eccentricity between tubes connected by right-angle coupler

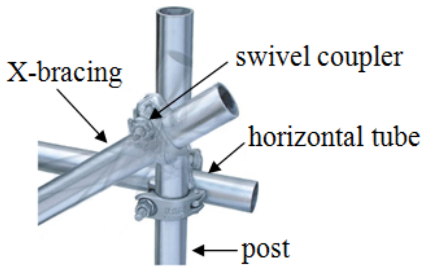

Figure 11. Connection mode of the X-bracing

Because the transverse and longitudinal tubes and the posts are continuous and no discontinuity in the members exists at the right-angle coupler location in practice, a three-dimensional beam element (BEAM188) was used to model the transverse and longitudinal tubes and the vertical posts. Figure 13 shows the modelling process. At the main node, two nodes N_{vHi} and N_{vLi} were defined along the z axis (i.e. the extension direction of the post) at a vertical separation of 150 mm. These two nodes belong to the post element. Node N_{Hi}, which belongs to the transverse horizontal tube element, was defined by shifting N_{vHi} 53 mm along the y axis (i.e. the extension direction of the longitudinal horizontal tube), and node N_{Li}, which belongs to the longitudinal horizontal tube element, was defined by shifting N_{vLi} 53 mm along the x axis (i.e. the extension direction of the transverse horizontal tube). To simulate the semi-rigid behaviour of the right-angle couplers, a spring-damper element (COMBIN14), which simulates the rotational restraint around the y axis (x axis), was added between node N_{vHi} (N_{vLi}) on the post and node N_{Hi} (N_{Li}) on the transverse horizontal tube (longitudinal horizontal tube). The coupling of these nodes was defined such that the nodes would have the same displacement in all directions and the same rotation around the vertical axis.

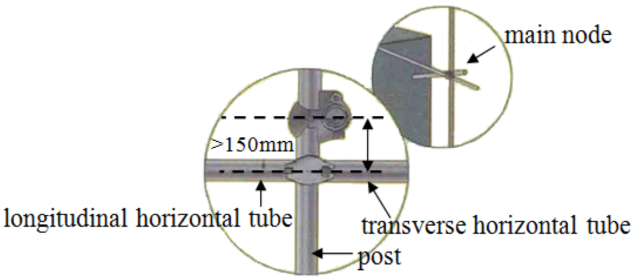

Figure 12. Connection mode of the main node.

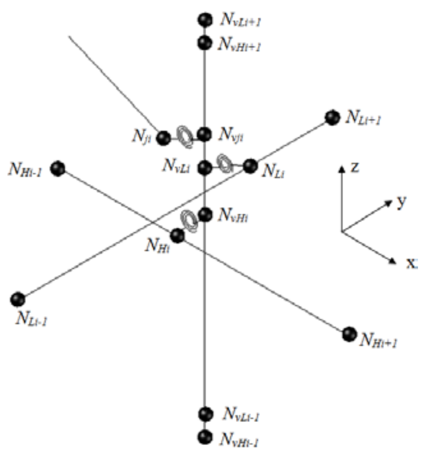

Figure 13. Establishment of nodes in FEA by considering the coupler eccentricity.

X-bracing members were considered to solely enhance the overall stiffness of the FSTFHS; hence, a three-dimensional link element (Link180) was used to model the X-bracing. To simulate the connection between the post and the X-bracing, two nodes N_{vji} and N_{ji} were defined at the location of the swivel coupler (Figure 11), where node N_{vji}, which belongs to the post element, was defined by shifting node N_{vLi} 150 mm along the z axis (i.e. the extension direction of the post), and node N_{ji}, which belongs to the X-bracing element, was defined by shifting node N_{vji} 53 mm along the x axis (when the X-bracing was set in the y–z plane) or the y axis (when the X-bracing was set in the x–z plane). The COMBIN14 element, which simulates the sliding constraint along the z axis, was added between nodes N_{ji} and N_{vji} with a spring constant of 1410 N/mm [24]. Coupling was defined for these two nodes in the remaining directions.

Four key points (two key points under the local area load condition), considered as the master nodes, were defined in the centroid of the designated loading areas atop the FSTFHS model. These points were located at positions corresponding to those of the hydraulic jacks in the tests. Beam-type constraints were added between the master nodes and each node on the top ho

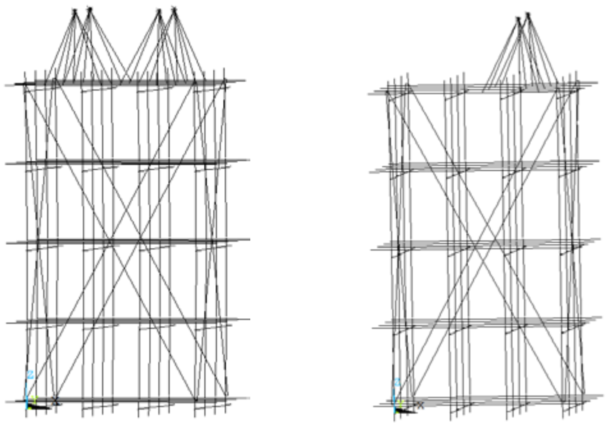

(a) Whole Area Load (b) Local Area Load

Figure 14. Finite Element Models of the FSTFHS by Considering the Upload Transference Eccentricity.

First, eigenvalue buckling analysis was conducted to obtain the elastic critical buckling loads as well as the failure modes for application in subsequent nonlinear analyses. Neither material nonlinearity nor geometric imperfections were considered in the eigenvalue buckling analysis because of the purely linearly elastic nature of the analysis. Subsequently, nonlinear analysis was conducted by considering the geometrical imperfections, geometric nonlinearity, and material nonlinearity. A concentrated load was incrementally applied to each key point on the designated loading area. This load was transformed into a uniform load through beam-type constraints and was transferred to the top horizontal steel tube until the FSTFHS became unstable or failure of the solution to converge occurred. The maximum load applied to the model was considered to be its strength. Material nonlinearity was accounted for using a perfect elastic–plastic material model, and the parameter values were determined through coupon tests. According to previous literature, the maximum imperfection allowed in practice is 0.05 m for a FSTFHS with height less than 10m [22]. Therefore, the first buckling mode identified from the eigenvalue buckling analysis with a maximum amplitude of 0.05 m was applied to the model as the initial geometric imperfection.

3. Results and Discussion

Table 1 lists the geometric properties, test specimen loading methods, and corresponding test results. For comparison, the table also lists the results of two FSTFHS prototype tests (PTS6 and PTS7) that we conducted before [19].

Table 1. Geometric parameters and test results for the full-scale specimens

NO.	Storey Height h (m)	Post Spacing $S_1 \times S_2$ (m × m)	Aspect Ratio H/B	Total Height (m)	Spans	Sweeping Staff Height (m)	X-bracing	Loading Method	P_{test} (kN)
TS1	1.8	1.3 × 1.3	2	8.00	3 × 3	0.3	None	Whole area load	8.58
TS2							Vertical	Whole area load	18.30
TS3								Local area load	16.08
TS4							Vertical + Horizontal	Whole area load	25.83
TS5								Local area load	18.33
PTS6	1.8	1.5 × 1.5	1.8	8.00	3 × 3	0.3	None	Whole area load	6.40
PTS7	1.5	1.2 × 1.2	1.6	8.00	4 × 4	0.3	None	Whole area load	12.22

Note: P_{test} stands for the strength of a single post obtained from the test. Symbols in Table 1 are shown in Figure 9.

The data listed in Table 1 [specifically, the comparison of TS1 (P_{test} = 8.58 kN) and PTS6 (P_{test} = 6.40 kN)] clarify that although increasing the post spacing could reduce the specimen aspect ratio, the strength of the FSTFHS without X-bracing would be reduced to some extent under the whole area load condition. In addition, when the storey height was large (e.g. ≈1.8 m), the aforementioned decrease was approximately 25 %. Therefore, to increase the strength of the FSTFHS, not only methods to reduce the aspect ratio but also other parameters such as the storey height, post spacing, and aspect ratio should be comprehensively considered in the design.

Furthermore, the data listed in Table 1 [specifically, the comparison of test TS1 (P_{test} = 8.58 kN) and PTS7 (P_{test} = 12.22 kN) as well as PTS6 (P_{test} = 6.40 kN) and PTS7 (P_{test} = 12.22 kN)] clarify that the FSTFHS strength would increase to some extent if both the storey height and post spacing are decreased.

For an FSTFHS without X-bracing, such as TS1, the typical failure mode was the global lateral buckling around the longitudinal weak axis [Figure 15(a)], similar to that for PTS6 [Figure 15(b)].

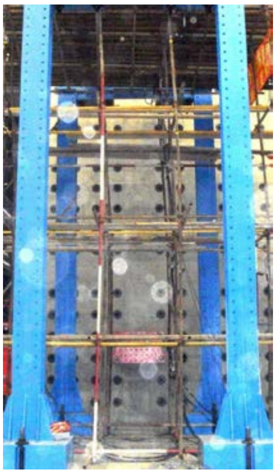

(a) TS1

(b) PTS6

Figure 15. Typical Failure Modes of an FSTFHS without X-bracing.

Table 2 lists the influence of the loading condition on the bearing capacity of the five FSTFHS test specimens. Compared with that of the whole area loading condition, the FSTFHS strength under the local area loading condition decreased to some extent. For the FSTFHS with all-around vertical X-bracing, the strength was reduced by 12.13 %, and for the FSTFHS with vertical and horizontal X-bracing (similar to the actual configuration in most construction projects), the strength was reduced by 29.04 %. For safety reasons, the FSTFHS test specimen without X-bracing was subjected to the whole area loading only.

Table 2. Effect of Loading Condition on the Bearing Behaviour of the FSTFHS.

Loading Condition	X-bracing		
	Vertical	Vertical + Horizontal	None
Whole area load P_{test_q}	18.30	25.83	8.58
Local area load P_{test_p}	16.08	18.33	–
$Diff1$ (%)	–12.13	–29.04	–

Note: 1. Unit: kN

2. P_{test_q} stands for the strength of a single post obtained from the test under whole area loading condition

3. P_{test_p} stands for the strength of a single post obtained from the test under local area loading condition

4. $Diff1 = \dfrac{P_{test\_p} - P_{test\_q}}{P_{test\_q}} \times 100\ \%.$

The failure modes of the tested FSTFHSs differed according to the applied loading condition. Figure 16(a) shows the typical deformed shape of TS2 under the whole area loading condition. All posts exhibited the same deformed shape, but only the posts in the two uppermost stories buckled evidently due to the vertical X-bracing and the action of the whole area uniform loading ($e_1 > e_2$ in the figure). Figure 16(b) shows the side view of the failure mode of TS3 under the local area loading condition. Part of the posts in the area close to the two working hydraulic jacks underwent large deformation ($e_3 > e_4$ in the figure). Figure 16(c) shows the plan view of the failure mode of TS3 under the local area loading condition. During buckling, the entire structure twisted anticlockwise ($e_5 < e_6$ in the figure). Moreover, the top horizontal tube bent [Figure 16(d)]. Thus, the typical failure mode of the FSTFHS under local area loading condition (e.g. local heaped load, which is common in construction sites) is the lateral buckling of part of the posts in the local loading area around the weak axis, accompanied by torsion of the entire structure and bending of the top horizontal tubes.

Table 3 lists the influence of X-bracing on the bearing capacity of the five FSTFHS test specimens. The X-bracing clearly increased the bearing capacity of the FSTFHS irrespective of the loading condition. Under the whole area loading condition, for the FSTFHS with all-around vertical X-bracing, the bearing capacity was approximately twice that of the FSTFHS without X-bracing. Under the same loading condition, by adding three X-bracing structures (one each at the top, middle, and bottom layers), the bearing capacities increased by 41.15 % and 13.99 % under the whole and local area loading conditions, respectively.

The comparison with our previous experimental and analytical results of the bearing capacity of FSTFHFS in [18, 19] indicates that the strength of the FSTFHS is lower than that of the FSTFHFS because of the difference in the load-transfer mechanisms in these two structures. In addition, the effect of the X-bracing on the bearing capacity of the FSTFHS was more evident than on that of the FSTFHFS (the effect varies with the geometric parameters and X-bracing configuration). These observations highlight the importance of X-bracing in enhancing the bearing capacity of the FSTFHS.

P_{FEA} is generally consistent in the full-scale test results with a maximum difference of −4.80 %, and the models can therefore be used in future parametric studies. The reasons attributed to the slight discrepancies could include variance in the rotational stiffness of couplers, variance in the mechanical properties of steel tubes, initial imperfections of the steel tubes, etc. Figure 17 shows the typical failure modes for TS1 and TS3 obtained through FEA, which were quite consistent with those observed in the full-scale tests. For the FSTFHS without X-bracing under whole area loading condition, global lateral buckling occurred around the longitudinal weak axis [Figure 17(a)]. In contrast, under local area loading condition, only the posts near the loading area underwent local large deformation [Figure 17(b)], accompanied by the twisting of the entire structure [Figure 17(c)] and bending of the top horizontal tubes [Figure 17(b)].

To investigate the influence of the eccentric axial load on the bearing capacity of the FSTFHS with various geometric properties, parametric studies were conducted on the developed FSTFHS models. The investigated parameters included storey height, post spacing, rotational stiffness of the couplers, and sweeping staff height. The primary layout of the finite element model included five spans along the longitudinal axis and five spans along the transverse axis using standard tubes of P48 mm × 3.5 mm in both directions. Table 5 lists the summary of the geometric dimensions used in the parametric studies.

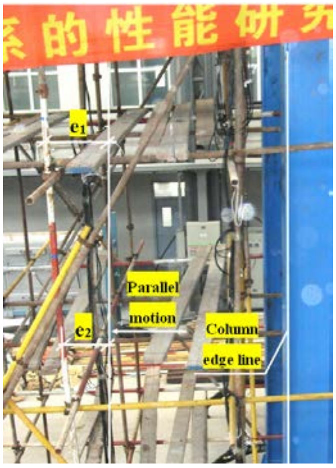

(a) Failure modes under the whole area load condition

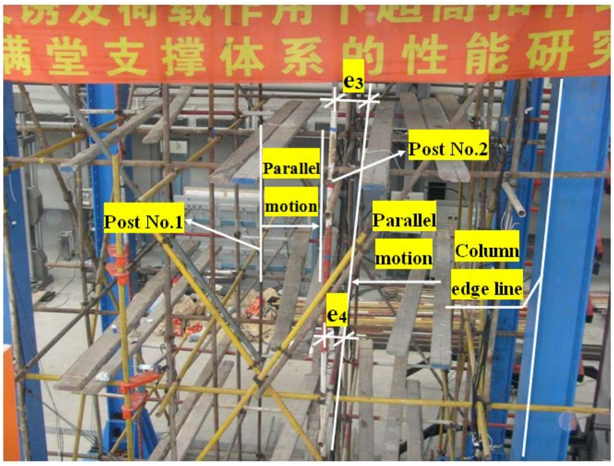

(b) Failure modes under the local area load condition (side view)

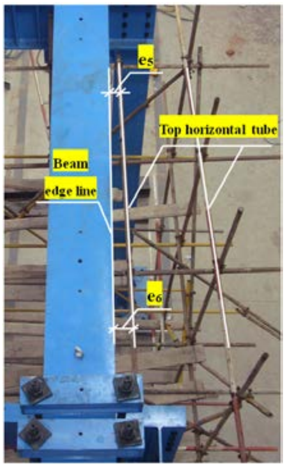

(c) Failure modes under the local area load condition (plan view)

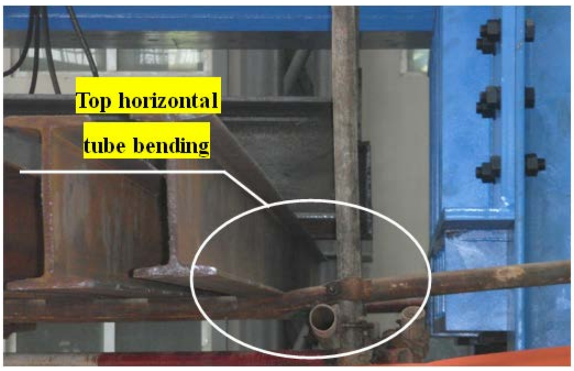

(d) Horizontal Tube Bending (Local Area Load Condition)

Figure 16. Typical failure modes of the FSTFHS under different loading conditions

Table 3. Effect of X-bracing on the bearing behaviour of FSTFHS.

X-bracing	Loading condition	
	Whole Area Load	Local Area Load
None (P_{test_w})	8.58	–
Vertical (P_{test_v})	18.30	16.08
$Diff1$	2.13 times	–
Vertical + Horizontal (P_{test_y})	25.83	18.33
$Diff2$	3.01 times	–
$Diff3$ (%)	41.15	13.99

Note: 1. Unit: kN

2. P_{test_w}, P_{test_v} and P_{test_y} all stand for the strength of the single post obtained from the test

3. $Diff1 = \frac{P_{test\_v}}{P_{test\_w}}$, $Diff2 = \frac{P_{test\_y}}{P_{test\_w}}$, and $Diff3 = \frac{P_{test\_y} - P_{test\_v}}{P_{test\_v}} \times 100\ \%$

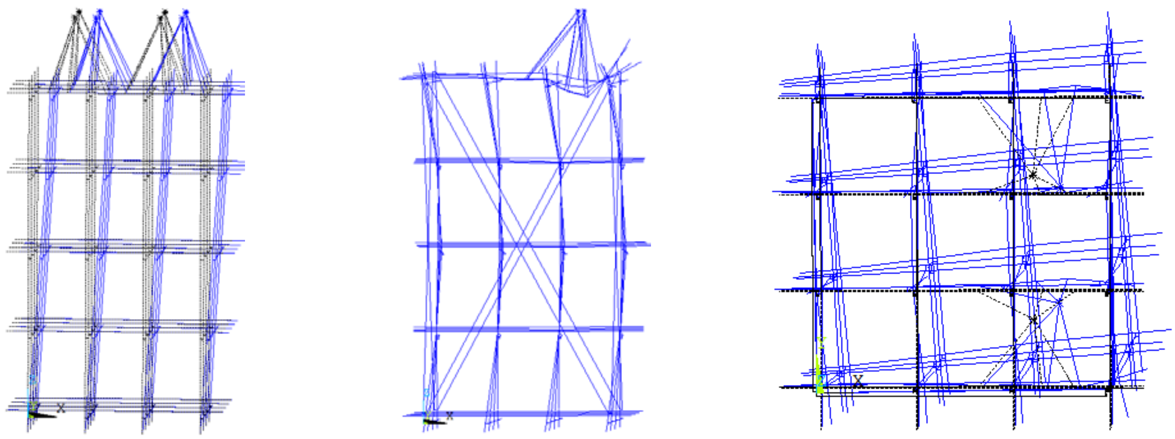

(a) Failure mode of the FSTFHS without X-bracing under the whole area load condition

(b) Failure mode of the FSTFHS with vertical X-bracing under the local area load condition (side view)

(c) Failure mode of the FSTFHS with Vertical X-bracing under the local area load condition (plan view)

Figure 17. Failure modes of the FSTFHS in FEA.

Table 4 lists the summary of the strength of single post P_{FEA} obtained through the nonlinear analyses and the experiments.

Table 4. Comparison of the results between FEA and the test.

NO.	Storey Height (m)	Post Spacing $S_1 \times S_2$ (m × m)	Aspect Ratio	X-bracing	Loading Condition	P_{test} (kN)	P_{FEA} (kN)	Diff (%)
TS1	1.8	1.3 × 1.3	2	None	Whole area load	8.58	8.24	–3.96
TS2				Vertical	Whole area load	18.30	17.80	–2.73
TS3					Local area load	16.08	15.97	–0.68
TS4				Vertical + Horizontal	Whole area load	25.83	24.59	–4.80
TS5					Local area load	18.33	18.06	–1.47

Note: 1. P_{test} and P_{FEA} stand for the strength of a single post obtained from the test and FEA, respectively.

2. $Diff = \frac{P_{FEA} - P_{test}}{P_{test}} \times 100\ \%$

Table 5. Study parameters on the effect of eccentric load.

NO.	Storey height (m)	Post Spacing $S_1 \times S_2$ (m×m)	Sweeping Staff Height (m)	Rotational Stiffness (kN·m/rad)	Total Height (m)
1	0.6–2.4	1.0 × 1.0	0.2	19	7.5–8.5
2	1.5	0.4 × 0.4–1.8 × 1.8	0.2	19	8.0
3	1.5	1.0 × 1.0	0.2	11–35	8.0

To further elucidate the influence of member eccentric axial loading, coefficient k, expressed in Eq. (1), was used to represent the adverse effect of the eccentric axial loading on the strength of the FSTFHS. The results clarified that the FSTFHS strength was reduced to some extent because of the eccentric axial loading on the members (Figure 18).

$$k = \left(1 - \frac{\text{Strength of single post with consideration of eccentric load}}{\text{Strength of single post without consideration of eccentric load}}\right) \times 100\,\%. \quad (1)$$

As the storey height increased, coefficient k decreased [Figure 18(a)], indicating a reduction in the adverse effects on the strength. When the storey height was 1.0–1.5 m, coefficient k evidently decreased. This could be because when the storey height is less than 1 m, numerous layers are necessary to fabricate the FSTFHS to a total erection height of 8 m, leading to the accumulation and expansion of the adverse effects of the layer-by-layer eccentric load transmission through the couplers. When the storey height increased, the required number of layers decreased, consequently ameliorating this effect. When the storey height was greater than 1.8 m, the effective length of the post was so large that its bearing capacity became very low, rendering the FSTFHS easily susceptible to failure due to eccentric axial loading and thus increasing k.

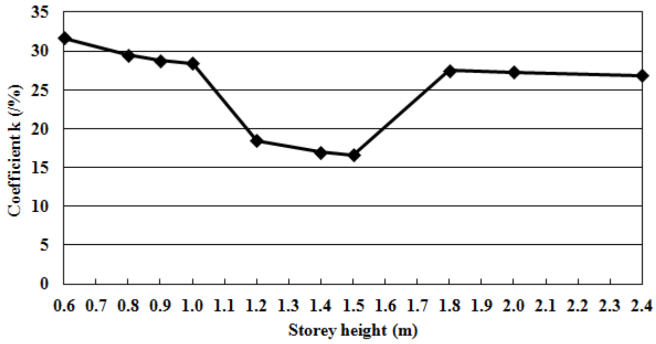

(a) Curve of influence coefficient k that varies with the storey height

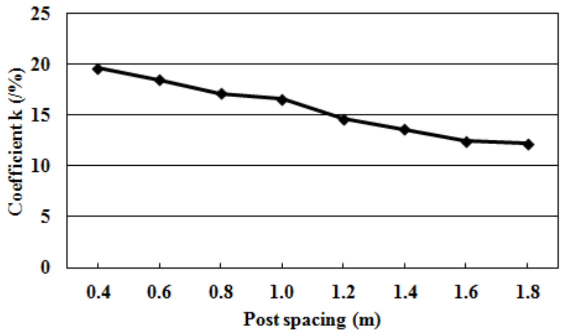

(b) Curve of influence coefficient k that varies with the post spacing

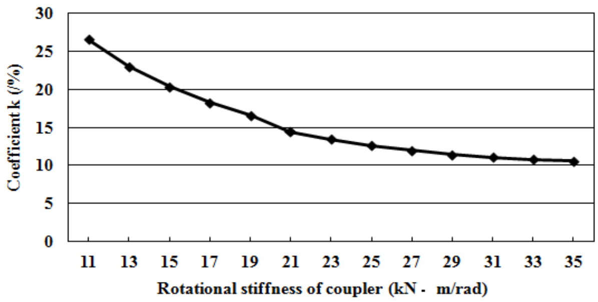

(c) Curve of influence coefficient k that varies with the coupler rotational stiffness

Figure 18. Parameter studies on the effect of member eccentric axial load.

Coefficient k decreased with post spacing [Figure 18(b)], probably because the reduced post spacing increased the height-to-width ratio, which in turn significantly reduced the bearing capacity of the FSTFHS. Moreover, such a configuration rendered the FSTFHS easily susceptible to failure due to eccentric axial loading.

Furthermore, k decreased with the coupler rotational stiffness [Figure 18(c)], indicating that the adverse effect of the eccentric axial loading on the members can be reduced to some extent by increasing the bolt-tightening torque to increase the rotational stiffness of the coupler, thus improving the FSTFHS bearing capacity.

4. Conclusions

A comprehensive research on the stability and strength of the FSTFHS with eccentric axial loading on the members was conducted through five full-scale tests as well as detailed FEAs. Therefore, combines with our previous results in [18–19, 25–28], the bearing capacity of FSTFHS that most commonly used in practical in China was studied, and the following conclusions are drawn:

1) The FSTFHS strength under local area loading condition is significantly lower than that under whole area loading condition.

2) The typical failure mode of the FSTFHS under local area loading condition is the lateral buckling of part of the posts around the weak axis near the local large loading area, accompanied by torsion of the entire structure and bending of the top horizontal tubes.

3) X-bracing evidently increases the bearing capacity of the FSTFHS regardless of the loading condition. The effect of X-bracing is stronger on the bearing capacity of the FSTFHS than on that of the FSTFHFS.

4) The FEA results are generally consistent with the test results, validating the FEA models for future applications.

5) The adverse effect of the eccentric axial loading on the strength of the FSTFHS decreases with the increase in the storey height, post spacing, and rotational stiffness of the couplers.

References

1. Chan, S.L., Zhou, Z.H., Chen, W.F., Peng, J.L., Pan, A.D. Stability Analysis of Semirigid Steel Scaffolding. Engineering Structures. 1995. Vol. 17. No. 8. Pp. 568–574.
2. Peng, J.L., Pan, A.D.E., Chan, S.L. Simplified Models for Analysis and Design of Modular Falsework. Journal of Constructional Steel Research. 1998. Vol. 48. No. 2–3. Pp. 189–209.
3. Peng, J.L., Pan, A.D.E., Chen, W.F. Approximate Analysis Method for Modular Tubular Falsework. Journal of Structural Engineering, ASCE. 2001. Vol. 127. No. 3. Pp. 256–263.
4. Peng, J.L., Pan, A.D., Rosowsky, D.V., Chen, W.F., Yen, T., Chan, S.L. High Clearance Scaffold Systems During Construction–1: Structural Modeling and Modes of Failure. Engineering Structure. 1996. Vol. 18. No. 3. Pp. 247–257.
5. Peng, J.L., Chen, K.H., Chan, S.L., Chen, W.T. Experimental and Analytical Studies on Steel Scaffolds under Eccentric Loads. Journal of Constructional Steel Research. 2009. Vol. 65. No. 2. Pp. 422–435.
6. Xiong, Y.Y., Xie, Y.X., Zhou, J.G. Discussion on Induced Load of Formwork with Fastener- Style Steel- Pipe Support System. Building Construction. 2004. Vol. 26. No. 1. Pp. 56–57.
7. Zeng, F.K., Liu, X.B., Hu, C.M., Yu, J., Zhang, T. Analysis of Two Kinds of Special Loads that High- formwork Supports System. Journal of Qingdao Agricultural University (Natural Science). 2007. Vol. 24. No. 4. Pp. 308–309.
8. Yuan, X.X., Jin, W.L., Liu, X., Lu, Z., Chen, T.M. Model for Fuzzy Risk Analysis of Fastener-style Tubular Steel Supported Scheme. Journal of Zhejiang University (Engineering Science). 2006. Vol. 40. No. 8. Pp. 1371–1376.
9. Hu, C.M., Jian, C.J., Duan, D.D., Fu, L.Y., Ren, W.J. Study of Time-varying Behavior of Multi-template Support System During Construction. Industrial Construction. 2016. Vol. 46. No. 3. Pp. 102–107.
10. Xie, N., Liang, R.Z., Wang, J.J. Occurrence of Human Errors in High Falsework and Influence on Structural Safety. Engineering Mechanics. 2012. Vol. 29. No. S1. Pp. 63–67.
11. Milojkovic, B., Beale, R.G., Godley, M.H.R. Determination of the Factors of Safety of Standard Scaffold Structures. Proceedings of the Third International Conference on Advances in Steel Structures. 2002. Vol. 1. Pp. 303–310.
12. Beale, R.G., Godley, M.H.R. Numerical Modeling of Tube and Fitting Access Scaffold Systems. Advanced Steel Construction. 2006. Vol. 2. No. 3. Pp. 199–223.
13. Beale, R.G. Scaffold Research – A Review. Journal of Constructional Steel Research. 2014. Vol. 98. Pp. 188–200.
14. Ao, H.F., Li, G.Q. Investigation of Overall Load-bearing Stability Capacity of Tube-and-coupler Scaffolds. Chinese Quarterly Mechanics. 2004. Vol. 25. No. 2. Pp. 213–218.
15. Yue, F., Yuan, Y., Li, G.Q., Ye, K.M., Chen, Z.M., Wang, Z.P. Wind Load on Integral-lift Scaffolds for Tall Building. Journal of Structural Engineering, ASCE. 2005. Vol. 131. No. 5. Pp. 816–824.
16. Liu, H.B., Zhao, Q.H., Wang, X.D., Zhou, T., Wang, D., Liu, J., Chen, Z.H. Experimental and Analytical Studies on the Stability of Structural Steel Tube and Coupler Scaffolds without X-bracing. Engineering Structures. 2010. Vol. 32. No. 4. Pp. 1003–1015.
17. Liu, H.B., Chen, Z.H., Wang, X.D., Zhou, T. Theoretical Analysis and Experimental Research on Stability Behavior of Structural Steel Tube and Coupler Falsework with X-bracing. Advanced Steel Construction. 2010. Vol. 6. No. 4. Pp. 949–962.
18. Lu, Z.R., Chen, Z.H., Wang, X.D., Guo, C., Liu, Q. Study of the Bearing Capacity of Fastener Steel Tube Full Hall Formwork Support using the Theory of Stability of Pressed Pole with Three-point Rotation Restraint. China Civil Engineering Journal. 2012. Vol. 45. No. 5. Pp. 104–113.
19. Lu, Z.R., Chen, Z.H., Wang, X.D., Liu, Q., Liu, H.B. Experimental and Theoretical Study of the Bearing Capacity of Fastener Steel Tube Hull-hall Formwork Support System. China Civil Engineering Journal. 2012. Vol. 45. No. 1. Pp. 49–60.
20. Chen, Z.H., Lu, Z.R., Wang, X.D., Liu, H.B., Liu, Q. Experimental and Theoretical Research on Capacity of Unbraced Steel Tubular Formwork Support Based on Sway Frame with Semi-rigid Connection Theory. Journal of Building Structures. 2010. Vol. 31. No. 12. Pp. 56–63.
21. Chinese Standards Institution, GB/T 228－2002: Metallic materials-Tensile testing at ambient temperature 2002.
22. Chinese Standards Institution, JGJ 130－2011: Technical Code for Safety of Steel Tubular Scaffold with Couplers in construction: 2011.
23. Chen, Z.H., Lu, Z.R., Wang, X.D. Numerical Analysis and Experimental Study of the Stiffness of Right Angle Couplers in Tubular Steel Scaffolds. China Civil Engineering Journal. 2010. Vol. 43. No. 9. Pp. 100–108.
24. Zheng, L.Q., Cai, X.F., Zhuang, J.P., Wu, J.L. Experimental Research on Anti-slipping Performance of Steel Pipe Joints with Swivel Coupler. Journal of Henan University (Natural Science). 2013. Vol. 43. No. 6. Pp. 711–715.
25. Lu, Z.R., Guo, C., Li, G.C., Chen, Z.H., Zhao, L., Yu, L. Testing Research on the Bearing Capacity of Fastener Steel Tubular Full Hall Formwork Scaffold. Construction Technology. 2016. Vol. 45. No. 15. Pp. 82–86.
26. Lu, Z.R., Guo, C., Li, G.C., Cao, S., Li, C.Y. Bearing Capacity of Bridge Full Hall Formwork Scaffold under Eccentric Load. Journal of Tianjin University (Science and Technology). 2016. Vol. 49, Supp1. Pp. 64–72.
27. Lu, Z.R., Guo, C., Yang, Y.M., Chen, Z.H. Study on the Effect of Coupler Eccentricity on Bearing Behavior of Steel Tubular Formwork Support. Industrial Construction. 2016. Vol. 46. No. 1. Pp. 140–146.
28. Lu, Z.R., Guo, C., Wen, Y.Q., Chen, Z.H., Liu, T., Cao, S. Study of Bearing Capacity of Fastener Steel Tubular Full Hall Formwork Support System under Eccentric Load. Journal of Dalian University of Technology. 2016. Vol. 56. No. 1. Pp. 20–27.

Contacts:

Zhengran Lu, 18842586845; luzhengranglovel@126.com

Guo Chao, 862424692693; guochaoglovel@126.com